Applied Catalysis B: Environmental 198 (2016) 180–188

Contents lists available at ScienceDirect

Applied Catalysis B: Environmental

journal homepage: www.elsevier.com/locate/apcatb

Photocatalytic CO_2 reduction promoted by a $CuCo_2O_4$ cocatalyst with homogeneous and heterogeneous light harvesters

Min Jiang, Yilin Gao, Zhaoyu Wang, Zhengxin Ding*

State Key Laboratory of Photocatalysis on Energy and Environment, College of Chemistry, Fuzhou University, Fuzhou 350002, PR China

ARTICLE INFO

Article history:
Received 2 April 2016
Received in revised form 19 May 2016
Accepted 22 May 2016
Available online 24 May 2016

Keywords:
CO_2 reduction
Photocatalysis
Cocatalyst
Spinel oxides
Electron transfer

ABSTRACT

Spinel $CuCo_2O_4$ nanoplates were synthesized through a solvothermal method coupled with a calcination treatment in air. The prepared $CuCo_2O_4$ samples were fully characterized by diverse physical and chemical techniques including powder X-ray diffraction (XRD), field emission scanning electron microscope (SEM), transmission electron microscope (TEM), X-ray photoelectron spectroscopy (XPS) and N_2 sorption measurement. The $CuCo_2O_4$ material was developed as an efficient, low-cost and stable cocatalyst to boost photochemical CO_2 conversion with $Ru(bpy)_3^{2+}$ as a homogeneous photosensetizer. The catalytic performance of the $CuCo_2O_4$ samples was evaluated toward visible-light-driven deoxygenative reduction of CO_2 to CO under mild conditions. Various parameters of the reaction system and the synthesis conditions of $CuCo_2O_4$ were investigated and optimized to maximize the catalytic performance of CO_2 reduction system. The stability and the reusability of the $CuCo_2O_4$ cocatalyst were examined. Moreover, the $CuCo_2O_4$ cocatalyst was further proved to be highly active to promote CO_2 photoreduction catalysed by CdS semiconductor as a heterogeneous light harvester, and markedly reinforced photocatalytic CO_2 reduction performance was achieved.

1. Introduction

The ever-increasing level of atmospheric CO_2 and the rapid-decreasing reserve of fossil fuels are two great challenges threatening the sustainable development of human society [1,2]. Intensive effort has thus been devoted to the development of efficient solutions to reduce CO_2 emission as well as the exploitation of clean alternatives to non-renewable sources [3–5]. As an abundant and inexhaustible resource, solar energy is considered as the most promising resource to operate endergonic fuel production reactions, such as the photocatalytic CO_2 reduction to generate energetic molecules (e.g. CO and CH_4), which not only contributes to the diminution of atmospheric CO_2 concentration, but also promises the production of valuable chemicals [6–10].

Since the innovative demonstration of photoelectrocatalytic reduction of CO_2 using semiconductor powders by Inoue and coworkers in 1979 [11], a wealth of materials have been developed to catalyse CO_2 conversion reactions with light, both in homogeneous and heterogeneous systems [12–14]. However, the achieved efficiency of CO_2 photoreduction is still far behind the need of practical application. To fulfil the crucial mission of CO_2 photofixation towards artificial photosynthesis with solar technology, further improvement in the efficiency of CO_2 photoconversion is thus unavoidable but highly challenging.

Among the examined approaches (e.g. ion doping [15], bandgap engineering [16], crystal engineering [17,18], nanostructuralization [19], sensitization [20], and Z-scheme construction [21,22]), the utilization of cocatalyst is considered as an effective method to improve CO_2 photoredox catalysis [23–25]. This is because cocatalyst can promote the transport of photogenerated electrons to suppress the recombination of charge carriers [26–28], as well as activate CO_2 molecules to lower the energy barrier of CO_2 reduction reaction [29], both of which can greatly elevate the efficiency of CO_2 photoreduction. Noble metals have long been employed as cocatalysts for photocatalytic CO_2 conversion with high activity and stability, but their low-abundance and high-price extremely disfavoured their large scale applications [30–32], and therefore, the exploitation of new cocatalysts made of inexpensive elements are more attractive [23,33–36].

Cobalt ions and cobalt-based complexes have been examined as efficient cofactors for supporting photochemical CO_2 reduction reactions. For instance, Lehn and co-workers have reported that Co^{2+} could significantly enhance photoreduction of CO_2 catalysed by $Re(bpy)(CO)_3Cl$ (bpy = 2,2-bipyridine) or $Ru(bpy)_3^{2+}$ [14].

* Corresponding author.
E-mail address: zxding@fzu.edu.cn (Z. Ding).

http://dx.doi.org/10.1016/j.apcatb.2016.05.055
0926-3373/

Fujita's group found that, with cobalt macrocyclic complexes as electron mediators, the activity and the selectivity of *p*-terphenyl-catalysed CO_2 photoreduction were prominently improved [37]. The results of these works disclosed that cobalt species are of particularly importance toward photochemical CO_2 reduction catalysis. Considering the weakness in separation and reuse of the homogeneous cofactors [38–41], we are interested in searching new cobalt-based heterogeneous cocatalysts for CO_2 photoreduction catalysis [42,43].

Here, we presented spinel $CuCo_2O_4$ nanoplates as an efficient, low-cost and stable cocatalyst to boost photocatalytic CO_2 reduction with $Ru(bpy)_3^{2+}$ and CdS to correspondingly serve as a homogeneous and a heterogeneous light harvester. The $CuCo_2O_4$ material was synthesized through a facile solvothermal-calcination coupled method, and was fully characterized by diverse physical and chemical techniques (e.g. XRD, SEM, TEM, XPS and N_2 sorption measurement). The catalytic performance of the $CuCo_2O_4$ samples was first evaluated for photochemical CO_2-to-CO conversion with $Ru(bpy)_3^{2+}$ as a visible-light photosensitizer under mild conditions. Various parameters of the reaction systems and the synthesizing conditions of $CuCo_2O_4$ were inspected and optimized. The stability and the reusability of the $CuCo_2O_4$ cocatalyst were examined. Moreover, the $CuCo_2O_4$ cocatalyst was further used to promoted CO_2 photoreduction catalysed by CdS semiconductor as a heterogeneous light harvester, and significantly enhanced CO_2 photoconversion performance was achieved.

2. Experimental

2.1. Materials

The chemical reagents used for synthesis of $CuCo_2O_4$ materials and photocatalytic CO_2 reduction reactions are all of analytical grade and used as received without further purification. Copper nitrate trihydrate [$Cu(NO_3)_2{\cdot}3H_2O$], cobalt-nitrate hexahydrate [$Co(NO_3)_2{\cdot}6H_2O$], cadmium sulfide (CdS) and triethylene glycol ($C_6H_{14}O_4$) were bought from Aladdin. 2,2′-bipyridine (bpy), $CoCl_2$ were purchased from Sigma. The organic solvents, including acetonitrile (MeCN), N, N-dimethylformamide (DMF), and dimethyl sulfoxide (DMSO) were purchased from China Sinopharm Chemical reagent Co. Ltd. Carbon dioxide gas, supplied by Fuzhou Lianzhong Industrial Gases Co. Ltd, is super grade purity (99.999%). The $^{13}CO_2$ (98% enriched) was purchased from Hess chemical gas center in Beijing.

2.2. Synthesis of photocatalysts

In the typical preparation of the $CuCo_2O_4$ samples, 2 mmol $Co(NO_3)_2{\cdot}6H_2O$ and 1 mmol $Cu(NO_3)_2{\cdot}3H_2O$ were dissolved in 35 ml deionized water and 5 ml triethylene glycol and magnetically stirred for 30 min [44,45]. After that, 15 mmol urea was added to the resulted mixture and was further vigorously stirred for another 30 min to get a homogeneous pink solution before transferred into a 50 ml Teflon-lined stainless steel autoclave. The autoclave was sealed and maintained at 120 °C for 12 h in an electric oven. After the temperature was cooled to room temperature naturally, the supernatant was removed, and the products were collected and washed with water and ethanol for several times. Then, the harvested $CuCo_2O_4$ precursors were dried at 60 °C for 12 h. Finally, the precursor were calcined at different temperatures (300, 400, 500, and 600 °C) in air for 4 h with a ramping rate of 1 °C min^{-1} to produce a series of $CuCo_2O_4$ samples, named as $CuCo_2O_4$-300, $CuCo_2O_4$-400, $CuCo_2O_4$-500, and $CuCo_2O_4$-600, respectively. For the clarity of discussion, the samples used for characterizations and photocatalytic reactions are the $CuCo_2O_4$-400 sample unless otherwise stated.

2.3. Characterization

A Bruker D8 Advance instrument (Cu Kα1 irradiation, λ = 1.5406 Å) was employed to collect the powder XRD patterns of the samples. The field emission SEM images were taken using a Hitachi New Generation SU8010 SEM with samples supported on an aluminium plate. The TEM images, the high-resolution TEM images and the selected area electron diffraction (SAED) patterns were obtained by JEOL model JEM 2010 EX instrument. A Micromeritics ASAP 3020 surface area analyser was used to determine the Brunauer- Emmett-Teller (BET) surface areas and the pore size distribution curve of the materials under liquid nitrogen temperature (77 K). The XPS spectra were acquired on a PHI Quantum 2000 XPS system with a monochromatic Al Kα source and a charge neutralizer.

In evaluation the catalytic CO_2 reduction performance of the samples, an Agilent 7820A gas chromatography equipped with a thermal conductivity detector (TCD) and a TDX-01 packed column was utilized to determine the yields of the products. The products generated from the $^{13}CO_2$ isotope experiment were analysed on a HP 5973 GC–MS instrument.

2.4. Photocatalytic test

The photocatalytic CO_2 reduction system was established with $CuCo_2O_4$ (4 umol) and $Ru(bpy)_3^{2+}$ (10 μmol) to act as a cocatalyst and a photosensitizer, dispersed in the mixed solution of TEOA/water/acetonitrile (1 ml/2 ml/3 ml) using an 80 ml Schlenk flask reactor. The CO_2 photoreduction catalysis was carried out under mild conditions (30 °C, 1 atm CO_2) using a 300 W Xe lamp with a 420 nm cutoff filter as the light source under energetically stirring. The $CuCo_2O_4$/CdS-catalysed photocatalytic CO_2 reduction system was constructed and operated under similar conditions (see Appendix A. Supplementary data for the details). After reacted for specific time, the generation of the products was calculated by the Agilent 7820A gas chromatography.

3. Results and discussion

3.1. Characterization of the samples

Firstly, powder XRD characterization was conducted to investigate the crystallographic structure of the $CuCo_2O_4$ samples synthesized under different calcination temperatures. As shown in Fig. 1, the XRD patterns of all the $CuCo_2O_4$ materials are indexed to the standard patterns of the spinel crystal structure (JCPDF card no. 78-2177). The diffraction peak indicated by the asterisk points to the presence of CuO in the prepared $CuCo_2O_4$ samples, which is consistent with the previously reported work [45]. It is clear that higher calcination temperature resulted in the $CuCo_2O_4$ samples with higher crystallinity, as mirrored by the intensity of the XRD patterns.

To examine the morphology of the $CuCo_2O_4$ samples, SEM and TEM measurements were carried out. From the typical SEM image (Fig. 2a), we can distinctly see that the prepared $CuCo_2O_4$ samples present a nanoplate microstructure with the thickness of *ca.* 100 nm. A further observation in the SEM photograph finds that there are numerous mesopores on each $CuCo_2O_4$ nanoplate, which was further confirmed by the TEM characterization (Fig, 2b). The lattice fringes in the high-resolution TEM image (Fig. 2c) together with the diffraction fringes in the SAED patterns (Fig. 2d) are well referenced to the interplanar spacing of the cubic $CuCo_2O_4$

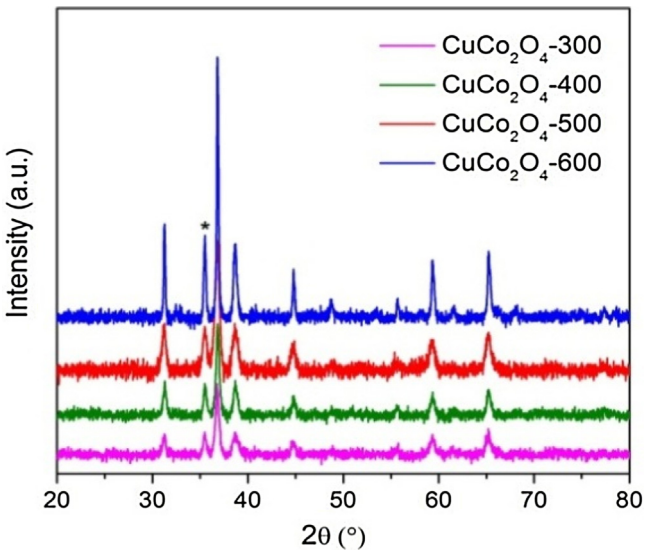

Fig. 1. XRD patterns of the $CuCo_2O_4$ samples synthesized under different calcination temperatures.

structure, reflecting the high crystallinity of the obtained materials using the applied synthesis protocol.

N_2 sorption measurements were performed to study the mesopore characteristics and the specific area of the $CuCo_2O_4$ samples. As shown in Fig. 3, the N_2 sorption isotherm of the $CuCo_2O_4$ material is assigned to type IV with a type H1 hysteresis loop, which obviously indicates the formation of mesopores in the $CuCo_2O_4$ nanoplates. The BET surface and the pore volume of the material is $32\,m^2\,g^{-1}$ and $0.064\,cm^3\,g^{-1}$, respectively. The pore size distribution curve (Fig. 3, Insert) further identifies the presence of mosepores in the materials with the pore size range of 2–14 nm and the average pore diameter of *ca.* 7 nm. In the procedure of synthesizing $CuCo_2O_4$ material (i.e. annealing at high temperatures in air), much CO_2 gas was released, which is considered as the main reason for the generation of these mesopores. In principle, the mesopores are very important for heterogeneous photocatalytic CO_2 reduction catalysis, not only exposing more catalytic active centres, but also promoting CO_2 absorption/activation, as well as favouring mass and charge transport. The results of N_2 sorption measurements further demonstrated that the calcination temperature greatly affected the BET surface area and the pore characteristics of the $CuCo_2O_4$ nanomaterials (Table 1), that is, with elevating the annealing temperature, the BET surface and pore

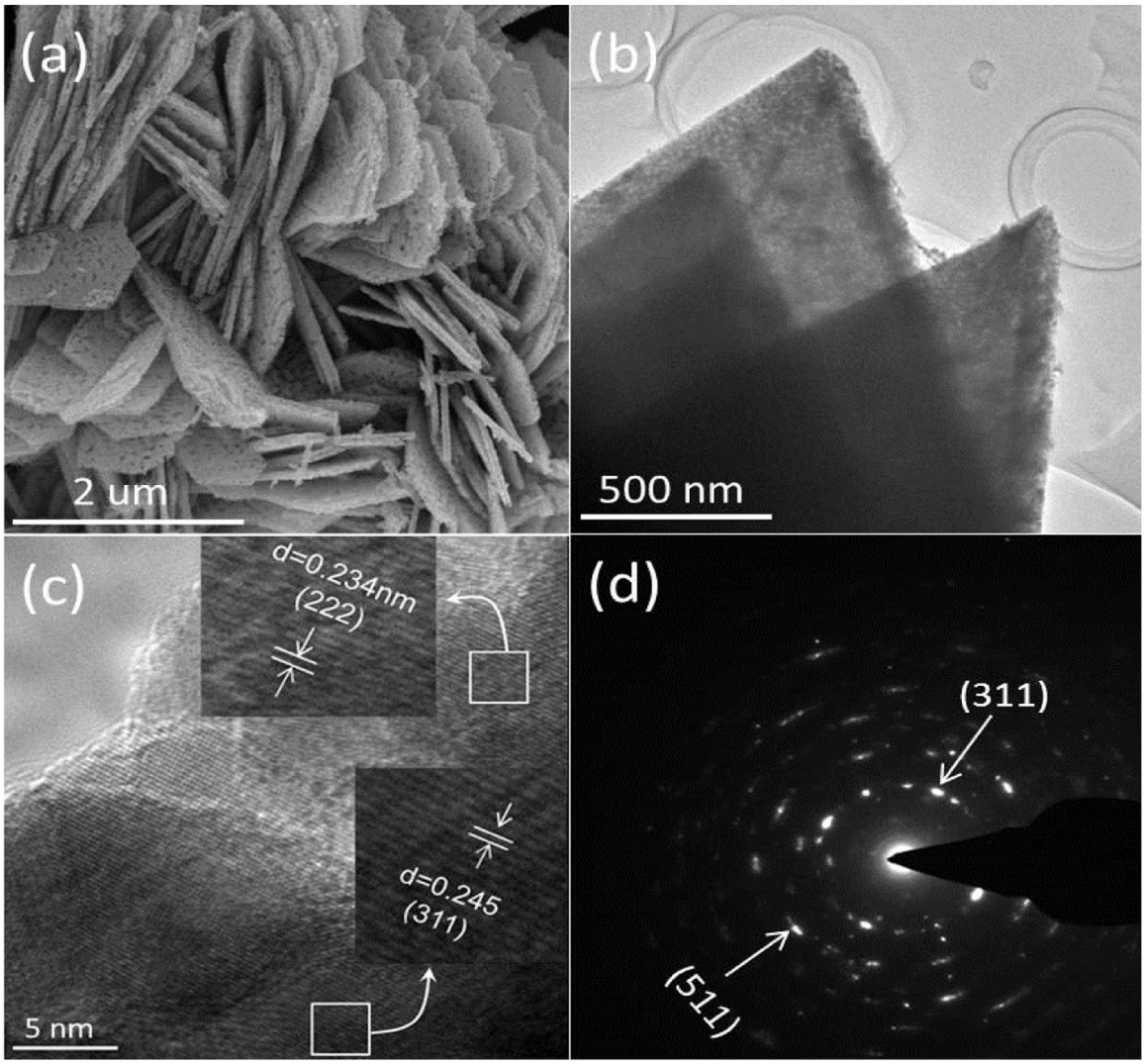

Fig. 2. (a), (b) SEM images, (c) high-resolution TEM image, and (d) SAED patterns of the $CuCo_2O_4$ nanoplates.

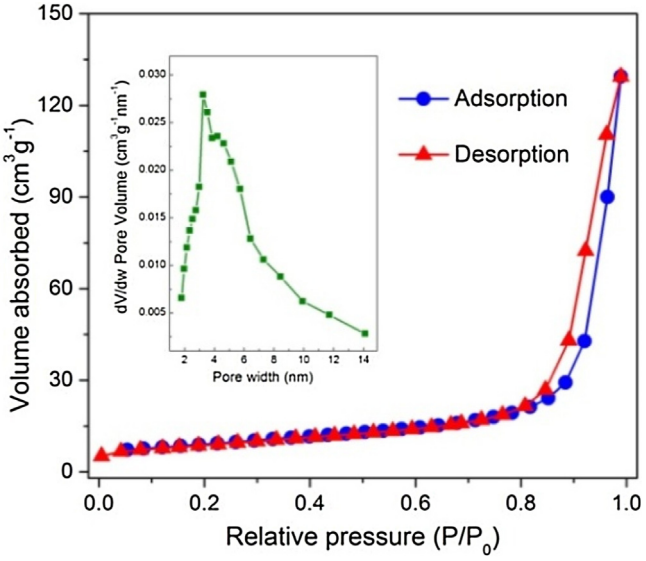

Fig. 3. N_2 sorption isotherms of the $CuCo_2O_4$ sample. Inset is the corresponding pore size distribution curve.

volume decreased obviously, but the average pore size increased, consistent with the results of reported work [46].

In order to gain the information about their chemical composition and the oxidation state of the component elements, the synthesized $CuCo_2O_4$ nanomaterials were further subjected to characterization by XPS. The general survey spectrum (Fig. 4a) displays the elemental signals of Cu, Co, O and C (originated from adventitious carbon species) without the assignment of other elements, implying the purity of the sample. In the complex high-resolution Co 2p spectrum (Fig. 4b), two prominent peaks at binding energy of 779.6 and 795.2 eV are assigned to the Co $2p_{3/2}$ and Co $2p_{1/2}$ spin-orbit peak, together with two obvious satellite peaks (denoted as "Sat." in the figure). Considering the energy gap between the main peaks and the satellite peaks, the Co 2p spectrum could be well-resolved into two spin-orbit doublet and four shakeup satellites by the Gaussian fitting method, pointing to the features of Co^{2+} and Co^{3+} cations [44]. The deconvoluted spectrum of Cu 2p displays two major Cu $2p_{3/2}$ and Cu $2p_{1/2}$ spin-orbit peaks at binding energy of 954.1 and 934.1 eV, and two satellite peaks (Fig. 3c), which suggests the oxidation state of Cu^{2+}. The O 1 s spectrum in Fig. 4d can be fitted into three photoelectron peaks positioned at 532.6, 530.9 and 529.4 eV, corresponding to the oxygen of physically adsorbed H_2O molecules, the oxygen of hydroxide ion, and the lattice oxygen in the spinel structure. The results of XPS measurements confirm the coexistence of solid-state Cu^{2+} and $Co^{2+/3+}$ in the spinel oxide $CuCo_2O_4$ structure [47,48], which may promise $CuCo_2O_4$ material with considerable opportunities for heterogeneous photoredox catalysis.

Table 1
Comparison of the BET surface area and the pore parameters of the $CuCo_2O_4$ materials synthesized at different calcination temperatures.

Samples	S_{BET} [a] ($m^2\ g^{-1}$)	Pore Volume [b] ($cm^3\ g^{-1}$)	Pore Size [c] (nm)
$CuCo_2O_4$-300	71	0.14	6.5
$CuCo_2O_4$-400	32	0.064	7.8
$CuCo_2O_4$-500	11	0.012	10.6
$CuCo_2O_4$-600	6	0.002	15

[a] S_{BET} = BET surface area.
[b] Total pore volume taken from the volume of N_2 adsorbed at ~P/P_0 = 0.99.
[c] Average pore size calculated using the desorption branch of the N_2 adsorption isotherms by the Barrett–Joyner–Halenda (BJH) method.

Table 2
Investigations on the reaction conditions.[a]

Entry	CO/μmol	H_2/μmol	Sel.$_{CO}$[b]/%
1	23	4.9	82.4
2[c]	0.1	0.6	14.3
3[d]	n.d.[e]	1.8	0
4[f]	n.d.	n.d.	/
5[g]	n.d.	n.d.	/
6[h]	n.d.	n.d.	/

[a] Reaction conditions: $CuCo_2O_4$ (4 μmol), $Ru(bpy)_3^{2+}$ (10 μmol), TEOA (1 ml), H_2O (2 ml), MeCN (3 ml), λ > 420 nm, 30 °C, 1 atm CO_2, 1 h.
[b] Sel.CO = mol CO/mol (CO + H_2).
[c] Without $CuCo_2O_4$.
[d] Using Ar to replace CO_2.
[e] n.d. = no detectable.
[f] Without Ru.
[g] In dark.
[h] Without TEOA.

3.2. Photocatalytic evaluation

The catalytic function of the $CuCo_2O_4$ material was first evaluated for supporting CO_2 photoreduction reaction with $Ru(bpy)_3^{2+}$ as a photosensitizer. Under the typical reaction conditions, 23 μmol CO and 4.9 μmol H_2 were produced from the chemical system (entry 1, Tabe 2), indicating the efficient photochemical reduction of CO_2 and protons, but CO_2 reduction reaction was dominant. No detectable hydrocarbons were formed in the liquid phase, and the distribution of reaction products was consistent with previously reported works [42,49–51]. The superior promotional effect of $CuCo_2O_4$ was further identified by the observation that the catalytic efficiency of CO_2-to-CO transformation reaction was greatly inhibited when it was removed from the reaction system (entry 2, Table 2).

Controlled experiments demonstrated that once the reaction occurred in an Ar atmosphere (entry 3, Table 2), the generation of CO was absolutely terminated, which thus reflected the origin of the formed CO was the CO_2 reactant. And to further confirm the carbon source of the CO generated, we carried out a ^{13}C-labeled isotropic experiment by using $^{13}CO_2$ to replace $^{12}CO_2$ under the same reaction conditions. From the results of mass spectroscope analysis (Fig. 5), the produced CO from the $^{13}CO_2$ isotope experiment was definitely assigned to ^{13}CO. The findings firmly proved that the $CuCo_2O_4$ material can indeed promote the photosplitting of CO_2 into CO in the chemical system.

When the photosensitizer $Ru(bpy)_3^{2+}$ was absent from the reaction system, no CO or H_2 was produced (entry 4, Table 2). In addition, the catalytic system was also inactive to generate any product without light illumination (entry 5, Table 2). These results revealed that the CO_2 conversion catalysis proceeded via a visible-light-induced photosensitization route, which was further validated by the studies on activity of the catalytic system as a function of the wavelength of incident light. As shown in Fig. 6, the trend of the yields of CO and H_2 matched well with the absorption spectrum of $Ru(bpy)_3^{2+}$ photosensitizer, not that of $CuCo_2O_4$ cocatalyst [14]. The observations revealed that the photochemical CO_2 reduction catalysis was actually started by visible-light-triggered excitation of the ruthenium dye, generating excited electrons to operate tandem photoredox reactions.

In order to effectively run the CO_2 photoreduction reaction, we then examined the catalytic activity of the reaction system with diverse solvents as the reaction medium. The results (Table S1) indicated that protic solvent (e.g. H_2O) repressed the activity of the system, while aprotic solvent (e.g. MeCN, DMSO, and DMF) favoured the evolution of CO and H_2. And eventually the catalytic system exhibited the highest activity when MeCN was the reaction medium, but the selectivity of CO was not satisfied.

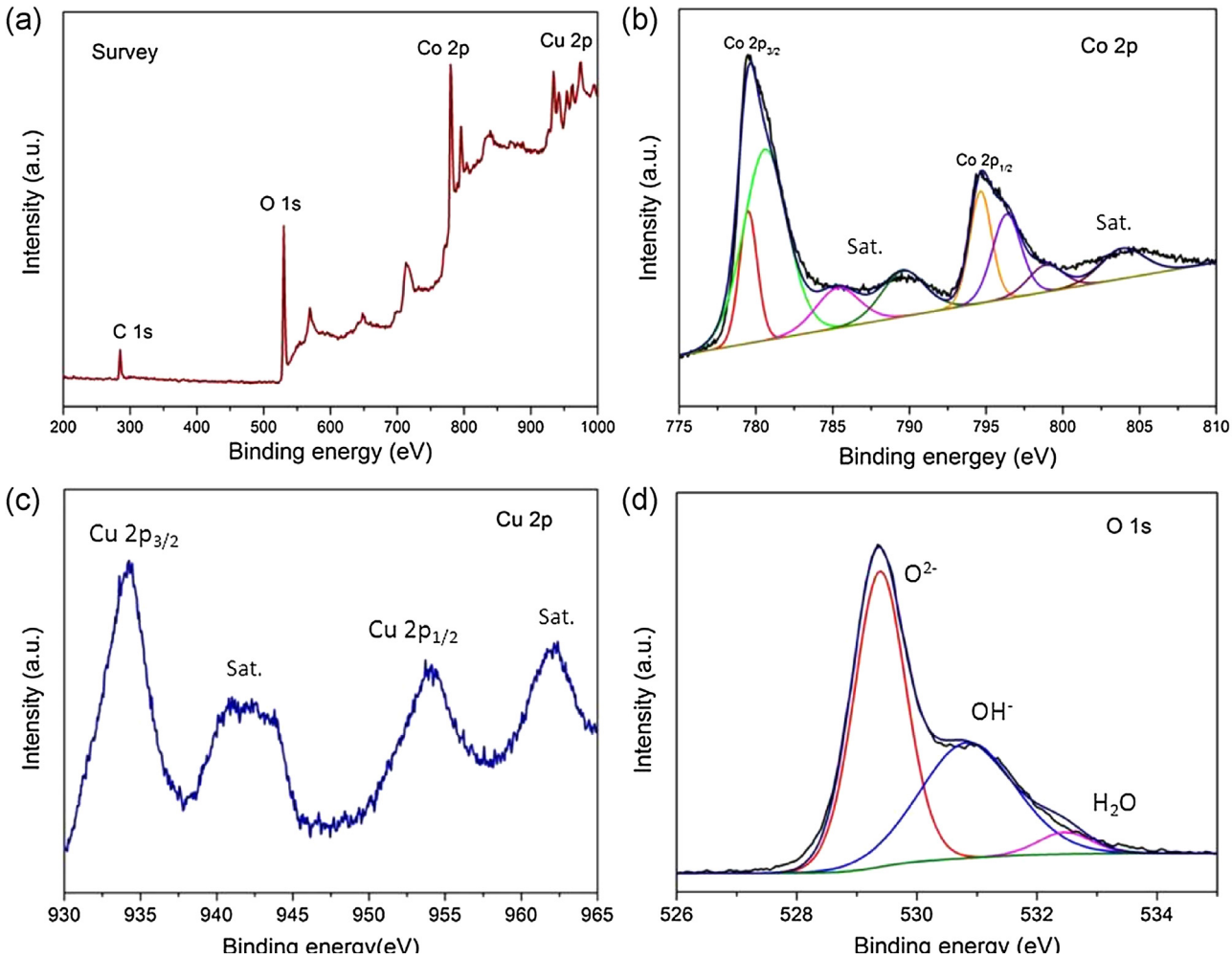

Fig. 4. XPS spectra of the $CuCo_2O_4$ sample: (a) survey spectrum and high-resolution spectra of (b) Co 2p, (c) Cu 2p, and (d) O 1s.

Indeed, the deoxygenative reduction of CO_2 to CO was disfavoured with H_2O as a single reaction medium, however, the participation of proper amount of H_2O often facilitated CO_2 conversion catalysis, owing that H_2O can not only accelerate the reaction kinetics, but also reduce the reaction barrier of CO_2 transformation reactions through the fashion of proton-coupled multielectron transport processes [14,52,53]. The mixtures of H_2O/MeCN was thus chosen as the reaction medium, and after optimizing the volumetric ratio of H_2O to MeCN (Table S2), the production of CO was substantially enhanced with the highest

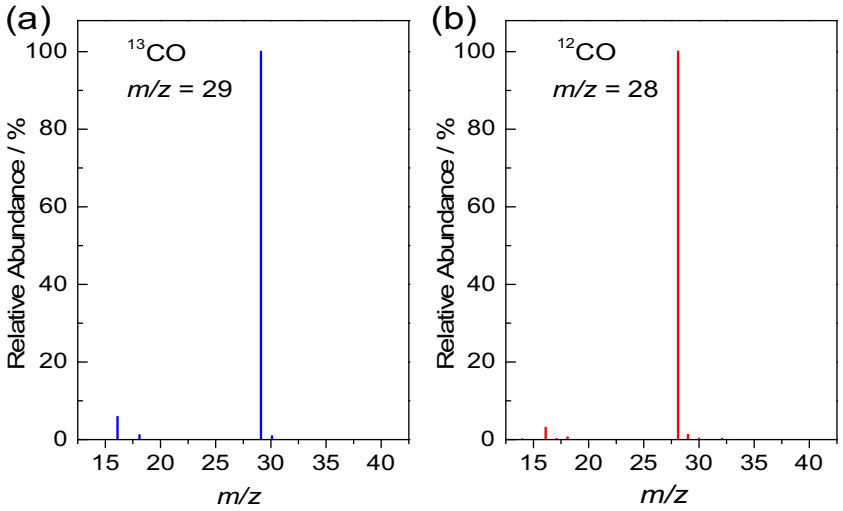

Fig. 5. Mass spectra of the CO generated from the reactions with (a) $^{13}CO_2$ and (b) $^{12}CO_2$ as the feedstock, respectively.

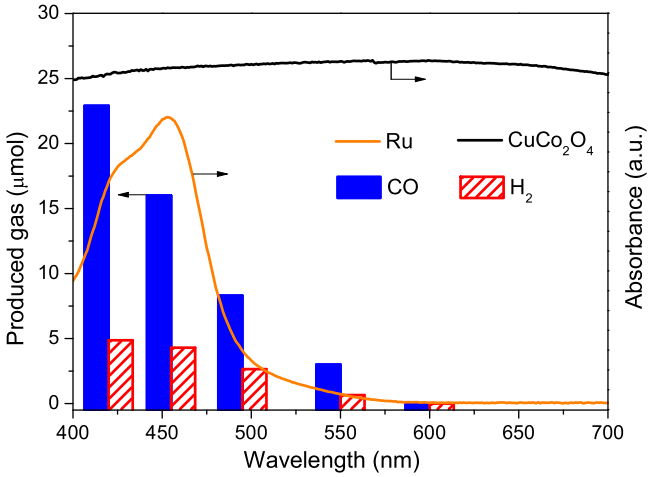

Fig. 6. Productions of CO/H_2 from the photochemical CO_2 conversion systems under irradiation light with different wavelengths. The lines are the absorption spectrum of $Ru(bpy)_3^{2+}$ and $CuCo_2O_4$. The wavelength of the incident light was adjusted by suitable long-pass cutoff filters.

CO generation rate of 22.9 μmol h^{-1} under the applied conditions. Additionally, by varying H_2O volume in the system, the ratio of CO to H_2 could be tuned widely from 1:4.2–4.7:1 in principle, which benefits the utilization of the evoluted gases as feedstocks to produce liquid fuels.

The effect of calcination temperature on the catalytic performance of the $CuCo_2O_4$ material was investigated and optimized. As presented in Fig. 7, the sample of $CuCo_2O_4$-300 exhibited a weaker activity than $CuCo_2O_4$-400. This is because the crystallinity of $CuCo_2O_4$-400 is higher (Fig. 1), enabling the better transport of photoinduced electrons. Further increasing the calcination temperature, the activities of $CuCo_2O_4$-500 and $CuCo_2O_4$-600 were however decreased, which was mainly attributed to the gradual diminution in specific surface of the samples (Table 1). The results revealed that both crystallinity and specific surface of the $CuCo_2O_4$ material greatly affected the catalytic activity, and the calcination temperature of 400 °C endowed the material with the highest catalytic function.

The generation of CO and H_2 from the $CuCo_2O_4$-promoted CO_2 photoreduction system as a function of irradiation time was studied. As shown in Fig. 8, the reaction system first exhibited high reaction rates for CO and H_2 generation, but then the reaction

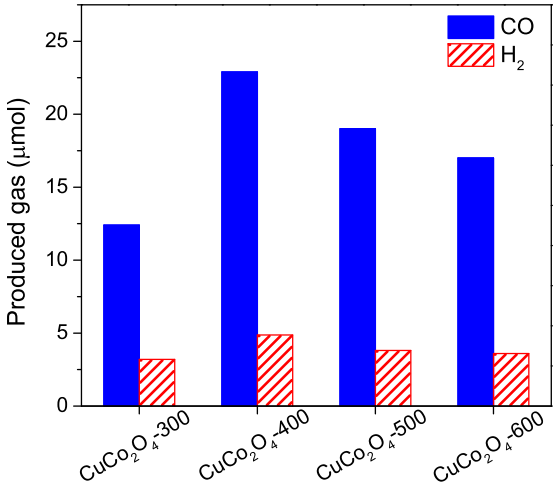

Fig. 7. Catalytic activities of the $CuCo_2O_4$ samples synthesized at different calcination temperatures.

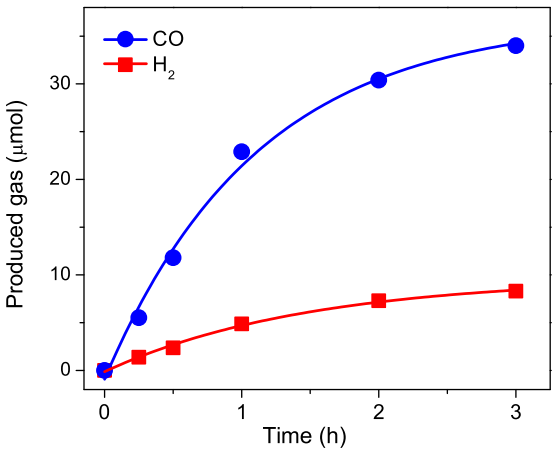

Fig. 8. Yields CO/H_2 produced from the photochemical CO_2 reduction system as a function of reaction time.

rates were decreased gradually, which was attributed to the photobleaching of the $Ru(bpy)_3^{2+}$ photosensitizer after limited catalytic runs [14,46,52]. In a reaction time of three hours, the accumulated production of CO/H_2 was 42 μmol, thus affording a catalytic turnover number (TON, with respect to $CuCo_2O_4$) of *ca.* 10 for the chemical system under optimized reaction conditions, and the achieved TON number is comparable to the results of some reported works [31,36].

After photocatalytic reactions, the $CuCo_2O_4$ cocatalsyt was separated from the reaction mixture, and then subjected to further characterizations and operations for evaluating stability of the $CuCo_2O_4$ materials in the hybrid chemical system. As can be seen in XRD patterns (Fig. 9) and the XPS spectra (Fig. 10), no noticeable alternations were detected in the crystal and chemical structures of the $CuCo_2O_4$ cocatalyst after photocatalytic reactions. The filtrated $CuCo_2O_4$ samples were further added to fresh reaction mixture again for supporting photochemical CO_2 reduction repeatedly, and it was found that the $CuCo_2O_4$ cocatalyst kept most of its original catalytic activity in five repeated runs (Fig. 11).

As above-demonstrated, the $CuCo_2O_4$ nanoplates material was developed to be a highly active and stable cocatalyst for promoting photochemical CO_2 reduction with $Ru(bpy)_3^{2+}$ as homogeneous photosensitizer. To explore the generality of the catalytic function of the $CuCo_2O_4$ cocatalyst, the CdS semiconductor was further selected as a heterogeneous light transducer to coorperate with

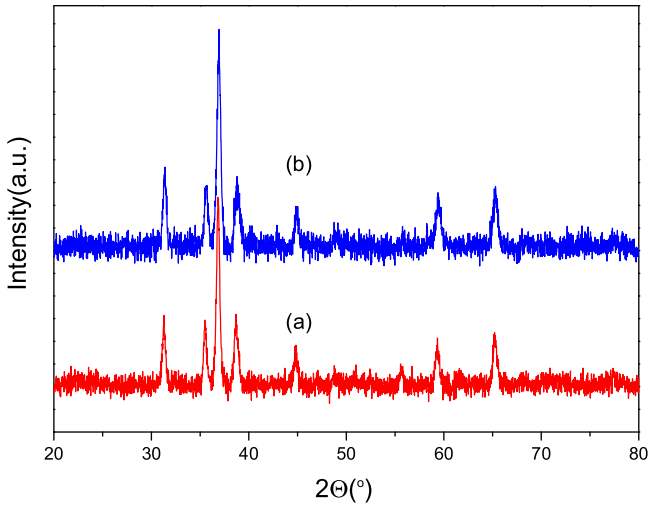

Fig. 9. XRD patterns of (a) used and (b) fresh $CuCo_2O_4$ samples.

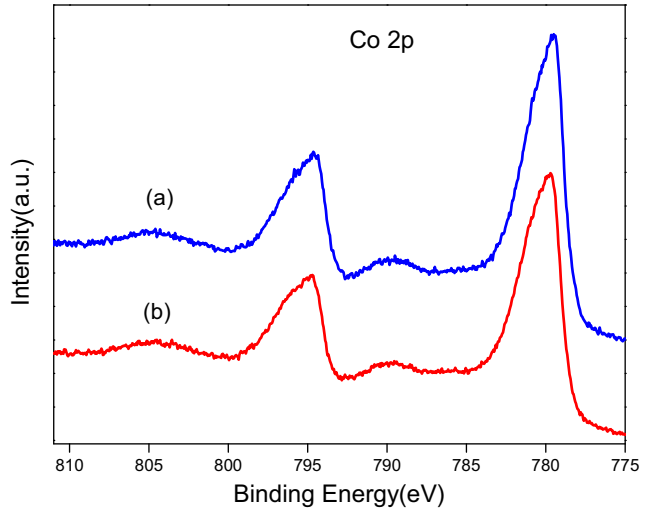

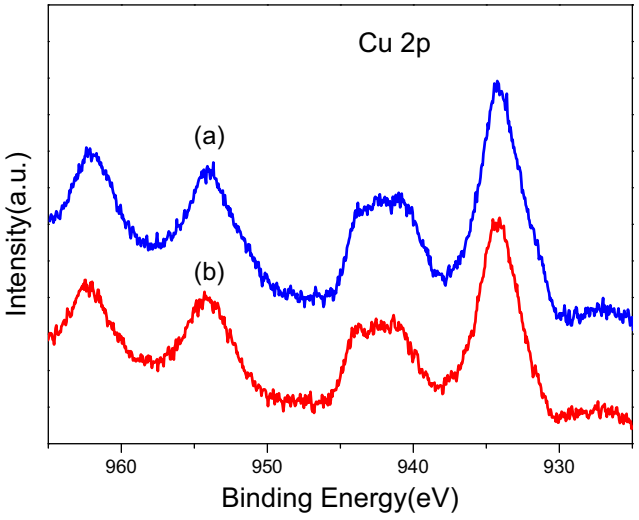

Fig. 10. XPS spectra of (a) used and (b) fresh $CuCo_2O_4$ samples.

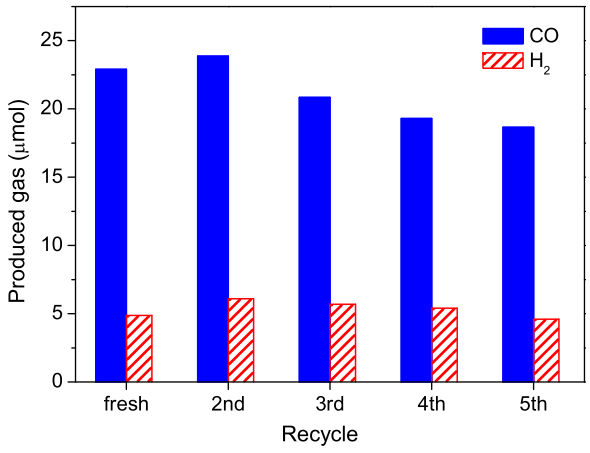

Fig. 11. Production of CO and H_2 in the stability test of the $CuCo_2O_4$ cocatalyst for photocatalytic CO_2 reduction.

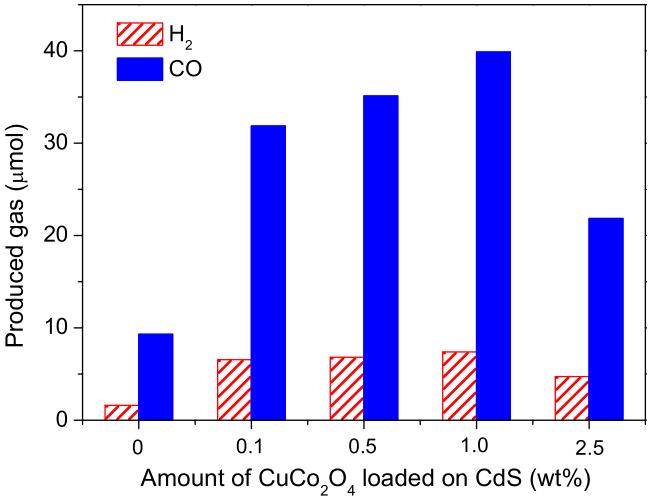

Fig. 12. Generation of CO and H_2 from the $CuCo_2O_4$/CdS catalysed photocatalytic CO_2 reduction system with different loadings of the $CuCo_2O_4$ cocatalyst.

$CuCo_2O_4$ to establish a new noble-metal-free $CuCo_2O_4$/CdS catalysed CO_2 reduction system under similar reaction conditions. The loading amount of the $CuCo_2O_4$ cocatalyst was optimized (Fig. 12), comparing with the pristine CdS photocatalysts, all the $CuCo_2O_4$/CdS samples exhibited obviously enhanced catalytic activity, and the 1.0 wt% $CuCo_2O_4$/CdS sample exhibited the highest catalytic activity with the CO generation rate of 40 μmol h^{-1} in the current CO_2 photoreduction system, disclosing the excellent cocatalytic effect of the $CuCo_2O_4$ material in the system. $^{13}CO_2$ isotope experiment was conducted for the $CuCo_2O_4$/CdS catalysed CO_2 reduction system, and the results (Fig. S2) confirmed that the carbon atom of the produced CO was stemmed from the CO_2 feedstock. Action spectrum of the CO_2 reduction using $CuCo_2O_4$/CdS photocatalyst was collected. As shown in Fig. S3, the trend of CO and H_2 evolution matched well with the optical absorption of the CdS photosensitizer, instead of that of the $CuCo_2O_4$ cocatalyst. This observation confirmed that the CO_2 photoreduction catalysis was indeed induced by light excitation of the CdS semiconductor.

The activity of the 1.0 wt% $CuCo_2O_4$/CdS sample was further inspected for reactions of different illumination times. As prolonging the reaction time, the yield of CO/H_2 increased gradually (Fig. 13), and in a-three-hour reaction, the total evolution of

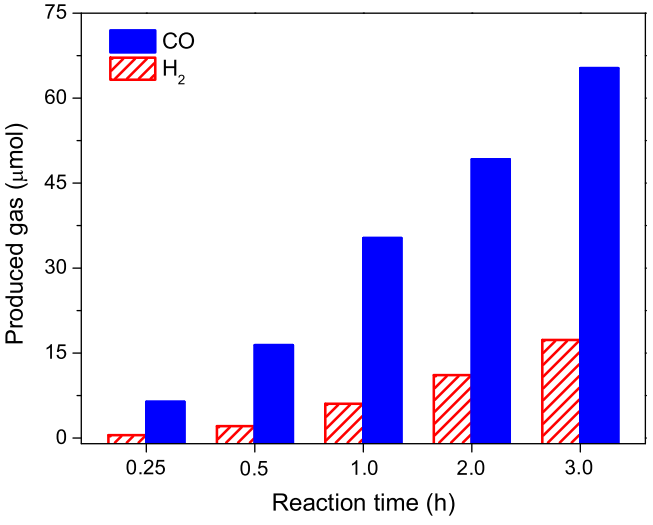

Fig. 13. Generation of CO and H_2 from the 1 wt% $CuCo_2O_4$/CdS photocatalytic CO_2 reduction system under visible light irradiations for different reaction times.

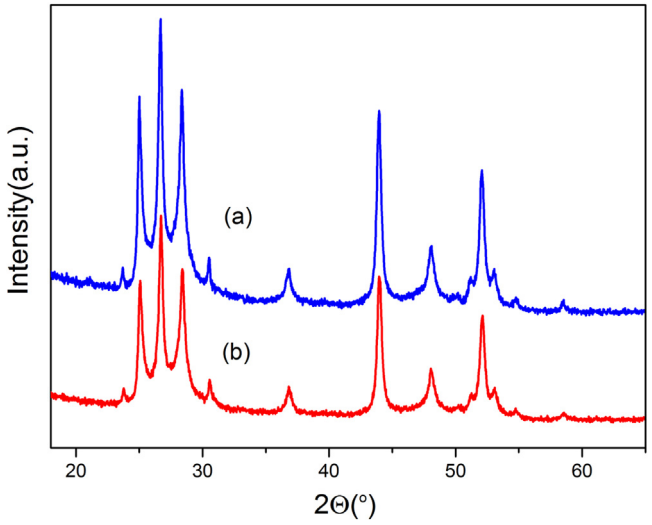

Fig. 14. XRD patterns of the $CuCo_2O_4$/CdS photocatalysts (a) before and (b) after photocatalytic CO_2 reduction reactions.

the products reached 82 μmol, corresponding to a TON of *ca.* 142 (with respect to $CuCo_2O_4$) for the system. To estimate its reusability, the $CuCo_2O_4$/CdS photocatalyst was separated after photocatalytic reaction, and then collected and reused for repeated reactions for four cycles. As shown in Fig. S4, the $CuCo_2O_4$/CdS photocatalyst kept most of its original catalytic activity for four repetitions of the operation, indicting the considerable reusability of the $CuCo_2O_4$/CdS photocatalyst. Furthermore, XRD characterization was further performed for the $CuCo_2O_4$/CdS samples after photocatalysis. As depicted in Fig. 14, the XRD patterns of used $CuCo_2O_4$/CdS photocatalyst matched well with that of the fresh sample, which reflected the stability of the $CuCo_2O_4$/CdS photocatalyst in the catalytic system. All these findings indicated that the $CuCo_2O_4$ cocatalyst was also stable and highly active to promote the photocatalytic reduction of CO_2 with CdS as a semiconductor light harvester, and noteworthily, the CO_2 photoreduction yield was greatly enhanced without the involvement of any noble metals.

4. Conclusion

In summary, the $CuCo_2O_4$ nanoplates material was prepared by a facile solvothermal-calcination method, and were fully characterized by diverse physical and chemical techniques. Initially, the $CuCo_2O_4$ nanoplates were developed as a low-cost, highly active and stable cocatalyst to promote photochemical CO_2 conversion with $Ru(bpy)_3^{2+}$ as a homogeneous photosensitizer under mild conditions. Various parameters of the CO_2 reduction system together with the synthesizing condition of the $CuCo_2O_4$ material were investigated and optimized, and the stability and reusability of the cocatalyst were also solidly confirmed. Moreover, a novel $CuCo_2O_4$/CdS photocatalytic CO_2 reduction system was further constructed and investigated. The $CuCo_2O_4$ cocatalyst effectively enhanced the CO_2-to-CO photoreduction catalysed by CdS as a heterogeneous light harvester, and greatly improved efficiency of CO_2 reduction was achieved (TON = 142) without the presence of any noble metals. Considering the enormous synthesis and modification engineering for fabricating desired spinel/semiconductor composite materials, this work will inspire intensive studies on solar-driven CO_2-to-fule conversion catalysis with cobalt-based spinel oxides (*e.g.* $CuCo_2O_4$) as the cocatalyst and semiconductors as light transducers.

Acknowledgements

This work is financially supported by the National Natural Science Foundation of China (21273039), the National Key Technologies R & D Program of China (2014BAC13B03), the National Basic Research Program of China (2014CB260406), and the Department of Education of Fujian Province in China (JB11001).

Appendix A. Supplementary data

Supplementary data associated with this article can be found, in the online version, at http://dx.doi.org/10.1016/j.apcatb.2016.05.055.

References

[1] F. Sastre, A. Corma, H. García, J. Am. Chem. Soc. 134 (2012) 14137–14141.
[2] S. Wang and X. Wang, *Angew. Chem. Int. Ed.* 55 (2016) 2308–2320.
[3] S. Wang and X. Wang, *Small* 11 (2015) 3097–3112.
[4] S. Wang, W. Yao, J. Lin, Z. Ding, X. Wang, Angew. Chem. Int. Ed. 53 (2014) 1034–1038.
[5] R. Kuriki, K. Sekizawa, O. Ishitani, K. Maeda, Angew. Chem. Int. Ed. 54 (2015) 2406–2409.
[6] W. Tu, Y. Zhou, Z. Zou, Adv. Mater. 26 (2014) 4607–4626.
[7] T.P. Yoon, M.A. Ischay, J. Du, Nature Chem. 2 (2010) 527–532.
[8] O.K. Varghese, M. Paulose, T.J. LaTempa, C.A. Grimes, Nano Lett. 9 (2009) 731–737.
[9] J.L. White, M.F. Baruch, J.E. Pander Iii, Y. Hu, I.C. Fortmeyer, J.E. Park, T. Zhang, K. Liao, J. Gu, Y. Yan, T.W. Shaw, E. Abelev, A.B. Bocarsly, Chem. Rev. 115 (2015) 12888–12935.
[10] Y. Izumi, Coordin. Chem. Rev. 257 (2013) 171–186.
[11] T. Inoue, A. Fujishima, S. Konishi, K. Honda, Nature 277 (1979) 637–638.
[12] A.J. Morris, G.J. Meyer, E. Fujita, Acc. Chem. Res. 42 (2009) 1983–1994.
[13] E. Fujita, Coordin. Chem. Rev. 185 (1999) 364–373.
[14] R. Ziessel, J. Hawecker, J.M. Lehn, Helv. Chim. Acta 69 (1986) 1065–1084.
[15] P.L. Richardson, M.L.N. Perdigoto, W. Wang, R.J.G. Lopes, Appl. Catal. B 126 (2012) 200–207.
[16] D.F. Wang, T. Kako, J.H. Ye, J. Phys. Chem. C 113 (2009) 3785–3792.
[17] G. Liu, C.H. Sun, H.G. Yang, S.C. Smith, L.Z. Wang, G.Q. Lu, H.M. Cheng, Chem. Commun. 46 (2010) 755–757.
[18] S.W. Liu, J.G. Yu, M. Jaroniec, J. Am. Chem. Soc. 132 (2010) 11914–11916.
[19] G. Kenanakis, N. Katsarakis, Appl. Catal. A 378 (2010) 227–233.
[20] O. Ozcan, F. Yukruk, E.U. Akkaya, D. Uner, Appl. Catal. B 71 (2007) 291–297.
[21] K. Sekizawa, K. Maeda, K. Domen, K. Koike, O. Ishitani, J. Am. Chem. Soc. 135 (2013) 4596–4599.
[22] Y. Sasaki, H. Nemoto, K. Saito, A. Kudo, J. Phys. Chem. C 113 (2009) 17536–17542.
[23] H. Tong, S. Ouyang, Y. Bi, N. Umezawa, M. Oshikiri, J. Ye, Adv. Mater. 24 (2012) 229–251.
[24] D. Sui, X. Yin, H. Dong, S. Qin, J. Chen, W. Jiang, Catal. Lett. 142 (2012) 1202–1210.
[25] T. Xie, D. Wang, L. Zhu, Mater. Chem. Phys. 70 (2001) 103–106.
[26] P. Pathak, M.J. Meziani, L. Castillo, Y.P. Sun, Green Chem. 7 (2005) 667–670.
[27] F. Solymosi, I. Tombacz, Catal. Lett. 27 (1994) 61–65.
[28] R. Gusain, P. Kumar, O.P. Sharma, S.L. Jain, O.P. Khatri, Appl. Catal. B 181 (2016) 352–362.
[29] K. Maeda, M. Higashi, D.L. Lu, R. Abe, K. Domen, J. Am. Chem. Soc. 132 (2010) 5858–5868.
[30] J. Hawecker, J.M. Lehn, R. Ziessel, J. Am. Chem. Soc. 9 (1983) 536–538.
[31] J. Qin, S. Wang, H. Ren, Y. Hou, X. Wang, Appl. Catal. B 179 (2015) 1–8.
[32] Y. Wei, J. Jiao, Z. Zhao, J. Liu, J. Li, G. Jiang, Y. Wang, A. Duan, Appl. Catal. B 179 (2015) 422–432.
[33] K. Maeda, R. Kuriki, M. Zhang, X. Wang, O. Ishitani, J. Mater. Chem. A 2 (2014) 15146–15151.
[34] F.Y. Wen, C. Li, Acc. Chem. Res. 46 (2013) 2355–2364.
[35] W.N. Wang, W.J. An, B. Ramalingam, J. Am. Chem. Soc. 134 (2012) 11276–11281.
[36] S. Wang, X. Wang, Appl. Catal. B 162 (2015) 494–500.
[37] J.H. Yang, D.G. Wang, H.X. Han, C. Li, Acc. Chem. Res. 46 (2013) 1900–1909.
[38] S. Matsuoka, K. Yamamoto, T. Ogata, M. Kusaba, N. Nakashima, E. Fujita, S. Yanagida, J. Am. Chem. Soc. 115 (1993) 601–609.
[39] L. Huang, D.C. Chen, Y. Ding, S. Feng, Z.L. Wang, M.L. Liu, Nano Lett. 13 (2013) 3135–3139.
[40] B. Cui, H. Lin, Y.Z. Liu, J.B. Li, P. Sun, X.C. Zhao, C.J. Liu, J. Phys. Chem. C 113 (2009) 14083–14087.
[41] J. Du, G. Zhou, H.M. Zhang, C. Cheng, J.M. Ma, W.F. Wei, L.B. Chen, T.H. Wang, ACS Appl. Mater. Interfaces 5 (2013) 7405–7409.
[42] S. Wang, Z. Ding, X. Wang, Chem. Commun. 51 (2015) 1517–1519.
[43] Z. Wang, M. Jiang, J. Qin, H. Zhou, Z. Ding, Phys. Chem. Chem. Phys. 17 (2015) 16040–16046.

[44] S. J. Li, Y. Xiong, Z. Liu, Y. Qian Ju, ACS Appl. Mater. Interfaces 5 (2013) 981–988.
[45] H. J. Cheng, Y. Yan, K. Lu, X. Qiu, J. Hou, L. Xu, X. Han, J. Liu, Y. Kim, J. Mater. Chem. A 3 (2015) 9769–9776.
[46] S. Wang, Y. Hou, X. Wang, ACS Appl. Mater. Interfaces 7 (2015) 4327–4335.
[47] Y. Sharma, N. Sharma, G.V.S. Rao, B.V.R. Chowdari, J. Power Sources 173 (2007) 495–501.
[48] W. Kang, Y. Tang, W. Li, Z. Li, X. Yang, J. Xu, C.S. Lee, Nanoscale 6 (2014) 6551–6556.
[49] Y. Liu, L. Cao, C. Cao, M. Wang, K. Leung, S. Zeng, T. Hung, C. Chung, Z. Lu, Chem. Commun. 50 (2014) 14635–14638.
[50] Z. Chai, Q. Li, D. Xu, RSC Adv. 4 (2014) 44991–44995.
[51] S. Wang, J. Lin, X. Wang, Phys. Chem. Chem. Phys. 16 (2014) 14656–14660.
[52] J.M. Lehn, R. Ziessel, J. Organomet. Chem. 382 (1990) 157–173.
[53] J. Schneider, H. Jia, J.T. Muckerman, E. Fujita, Chem. Soc. Rev. 41 (2012) 2036–2051.